Watt-level Pr^{3+}:YLF deep red laser pumped by a fiber-coupled blue LD module or a single-emitter blue LD

Miaomao He (何苗茂)[1], Sheng Chen (陈 升)[1], Quanxin Na (纳全鑫)[1], Shaojuan Luo (罗劭娟)[1], Haiyong Zhu (朱海永)[3], Ying Li (李 瑛)[1,2], Changwen Xu (许长文)[1,2,*], and Dianyuan Fan (范滇元)[1,2]

[1]*International Collaborative Laboratory of 2D Materials for Optoelectronics Science and Technology of Ministry of Education, Institute of Microscale Optoelectronics, Shenzhen University, Shenzhen 518060, China*

[2]*Engineering Technology Research Center for 2D Material Information Function Devices and Systems of Guangdong Province, Shenzhen University, Shenzhen 518060, China*

[3]*College of Electrical and Electronic Engineering, Wenzhou University, Wenzhou 325035, China*

**Corresponding author: chwxu@szu.edu.cn*

Received September 10, 2019; accepted October 16, 2019; posted online December 23, 2019

A power-scaled laser operation of Pr:$YLiF_4$ (YLF) crystal at 720.9 nm pumped by a 443.6 nm laser diode (LD) module was demonstrated. The 20 W module was used to pump the Pr:YLF crystal, and a maximum output power of 3.03 W with slope efficiency of 30.04% was obtained. In addition, a 5 W blue LD was also used to pump the Pr:YLF laser, and a maximum output power of 0.72 W was obtained at room temperature. The output power was limited by the wavelength mismatch between the single-emitter LD and the absorption peak of the crystal.

Keywords: rare earth and transition metal solid-state lasers; visible lasers; diode-pumped lasers.
doi: 10.3788/COL202018.011405.

Visible lasers are enthralling due to the characteristic that can be directly perceived by the human eye. Visible lasers have been widely used in medical imaging, optical storage, laser projection, and the like. It has been proved that many trivalent rare-earth ions (RE^{3+}) could directly generate a visible laser by stimulated radiant energy[1]. The trivalent praseodymium ion (Pr^{3+}) is considered to be one of the most efficient rare-earth ions for direct emission of a visible laser. It exhibits various emission lines throughout the visible spectral range, and their emission cross sections are larger than that of other RE^{3+} in the $LiLuF_4$ (LLF) host[1].

A variety of Pr^{3+}-doped crystals directly generating visible lasers have been reported, for example, $YLiF_4$ (YLF)[2–16], $YAlO_3$ (YAP)[6,17–19], BY_2F_8 (BYF)[8], LLF[20], $LaMgAl_{11}O_{19}$ (LMA)[21], $Sr_{0.7}La_{0.3}Mg_{0.3}Al_{11.7}O_{19}$ (ASL)[22], etc. Pr:YLF is the most established laser crystal for the direct generation of visible laser since it exhibits a longer upper state lifetime and smaller phonon energy. In the twentieth century, the pump sources used for the Pr^{3+} lasers were the dye laser[23], flash-lamp[2], and argon ion laser[3], but they were not suitable as a pump for the Pr^{3+} visible laser due to low efficiency and complicated structure. In the past two decades, frequency-doubled optically pumped semiconductor lasers (2ω-OPSLs) and gallium nitride (GaN) laser diodes (LDs) have been widely employed as pump sources for Pr^{3+} visible lasers[8,9]. Although the 2ω-OPSL pump sources operating in a blue spectral range have excellent beam quality, they still have some disadvantages such as high price, cumbersome structure, and limited power. Thanks to the development of the blue LD, in 2004, Richter *et al.* used a GaN LD to pump a Pr:YLF crystal to produce a red laser for the first time[4], to the best of our knowledge. Moreover, the fiber-coupled blue LD module or single-emitter LD as a pump source will help to reduce system complexity and facilitate the development of miniaturized lasers. In 2018, Tanaka *et al.* demonstrated laser operation at 640 and 607 nm, and the maximum output power was 6.7 and 3.7 W, respectively, by four LDs double-ended pumped. Meanwhile, a fiber-coupled module with more than 20 W was also used for the first time, to the best of our knowledge, to pump Pr:YLF to obtain an output power of 3.4 W at 640 nm[12].

The 720.9 nm wavelength is among the strongest emission peaks of Pr:YLF crystal. The 720.9 nm deep red laser has practical applications in many fields. For example, it can be used to observe the populations and dynamics of guanine radicals in DNA strands[24], because this wavelength overlaps with the maximum absorption peak of hydrated electrons[25], as a two-photon fluorescent dye excitation light source in some live cell imaging experiments[26], and an ultraviolet laser by frequency doubling can be used for food safety testing[27]. As far as we know, the maximum continuous-wave (CW) output power at 720.9 nm was 2.5 W by 2ω-OPSLs (479 nm) pumped[5], while 1 W maximum output at 720.9 nm was obtained from four blue single-emitter LDs (444 nm) pumped Pr:YLF[15]. Up to now, the output performance at 720.9 nm is still at a lower level than those of the Pr:YLF visible laser in other bands. Therefore, the deep red laser of Pr:YLF still has the potential for power scalability, with a higher power pump source or optimized relevant parameters.

In this Letter, we report a deep red laser of Pr:YLF operation at 720.9 nm with two different pump sources, a 443.6 nm LD module of more than 20 W incident pump

power and a 5 W blue LD. The module was used to pump Pr:YLF crystals and a maximum output power of 3.03 W, corresponding to slope efficiency of 30.04%, was achieved. For the module pumping, the CW output power was pump limited. Moreover, a 5 W blue LD was also used as pump source, and the maximum output power of 0.72 W was obtained at room temperature.

A stable high-power laser output of Pr:YLF at 720.9 nm was demonstrated by employing a fiber-coupled blue-light LD module pump source. In the case of high-power pumping, the heat accumulation inside the crystal is severe, and heat dissipation measurements must be taken to protect the laser crystal during the experiment. A 0.5 at.% crystal was damaged, when incident pump power exceeded 20 W at non-lasing, and the diameter of the pump spot was set to 300 μm[12]. The Pr:YLF crystal has polarization dependent absorption spectra, and the absorption peaks at 444 nm, 469 nm, and 479 nm in the π direction are much higher than the ones in the σ direction[28]. Therefore, *a*-cut 0.3 at.% Pr:YLF crystals were adopted in the experiment. The crystals have dimensions of 3 mm × 3 mm × 10 mm and 3 mm × 3 mm × 6 mm. The 3 mm × 3 mm facets were polished to laser quality and antireflection coated in the range of 430−490 nm and 720.9 nm. For waste heat removal, the laser crystals were enclosed by indium foil and mounted in a water-cooled copper block. The circulating water temperature was kept at 15°C. The pump source can provide maximum output power of 22.5 W. The fiber core diameter was 200 μm, and the numerical aperture (NA) was 0.22. The output power curve of the pump source and the spectrum at its maximum output are shown in Fig. 1. At the highest output power, the center wavelength of the pump source was 443.6 nm, and the full width at half-maximum (FWHM) was 1.8 nm.

The schematic experimental setup with the 443.6 nm LD module is depicted in Fig. 2. The laser resonator was a common plano-concave cavity. The pump light was coupled into the laser crystal through two doublets (F1 and F2). The input mirror (IM) was a plane one, antireflection coated for the pump wavelength ($T > 98\%$ from

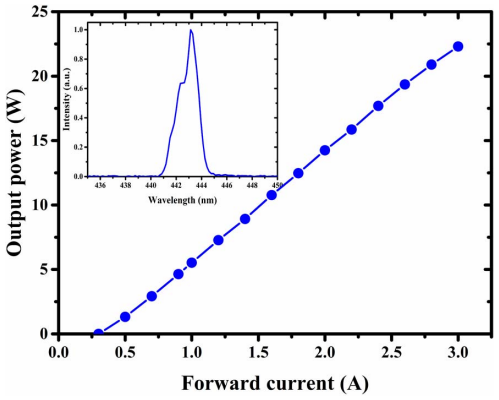

Fig. 1. Power characteristic of LD module and the output spectrum at the maximum output power.

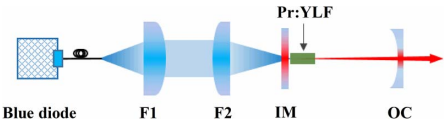

Fig. 2. Schematic diagram of Pr:YLF laser at 720.9 nm pumped by the 443.6 nm LD module.

440 nm to 445 nm), and high reflection coated for the laser wavelength ($R > 99.9\%$ at 720 nm). The output coupler (OC) was a plano-concave one. OCs with different radii of curvature (ROCs) and transmission were used for the experiments, respectively. The laser output power was measured by a power meter (Huayi Optics, TP50-HP-19).

The maximum tensile stress on the surface of the crystal can be estimated according to the following equation[29]:

$$\sigma_{\max} = \alpha_T E \frac{\eta_{\text{th}} P_{\text{in}} \alpha}{4\pi K}\left[1 - \frac{1}{2}\left(\frac{\omega_p}{r_b}\right)^2\right], \tag{1}$$

where α_T is the thermal expansion coefficient (13.3×10^{-6} K^{-1} for the *a* axis of YLF), K is the thermal conductivity (5.8 $\text{W} \cdot \text{m}^{-1} \cdot \text{K}^{-1}$ for the *a* axis of YLF)[30], E is Young's modulus (85 GPa for YLF), P_{in} is the incident pump power, ω_p is the radius of the pump beam spot in the gain crystal, α is the absorption coefficient (1.2 cm^{-1} for the 0.3 at.% YLF), r_b is the circumferential circle radius of the Pr:YLF square rod (~2.12 mm), and η_{th} is the thermal loading. For simplicity, only the quantum defect heating, corresponding to $1 - \eta_{\text{Stokes}}$, was taken into account to calculate the tensile stress. The calculated maximum tensile stress was 13.8 MPa if the pump spot diameter was set to 200 μm. The fracture limit of YLF was 40 MPa[29], which is much larger than the calculated values. In the first place, two doublets (F1 and F2) with focal lengths of 50 mm and 50 mm were used, resulting in a 200 μm pump spot. However, the 0.3 at.% crystal fractured at an incident pump power of 20.16 W. When two doublets (F1 and F2) with focal lengths of 50 mm and 80 mm were used, resulting in a 320 μm pump spot in the crystal, no fracture was found, even at the maximum incident pump power.

The maximum incident power applied to the crystal was 20.55 W, due to the loss by F1, F2, and IM. The 6-mm-long Pr:YLF crystal was tested first. When the crystal did not lase, the maximum absorbed pump power was measured to be 9.49 W, corresponding to an absorption efficiency of 44%. OCs with ROCs of 50 mm and different transmissions were used. The laser output curve of the 6-mm-long Pr:YLF crystal is shown in Fig. 3 (top). For the 5% OC, the threshold absorbed power was 1.54 W, and the maximum output power of 2.42 W, with slope efficiency of 33.20%, was obtained. For the 1.8% OC, the threshold absorbed power was 0.79 W, and the maximum output power of 1.5 W was obtained at the absorbed pump power of 6.76 W. When the absorbed pump power exceeded 6 W, a higher-order transverse mode was onset.

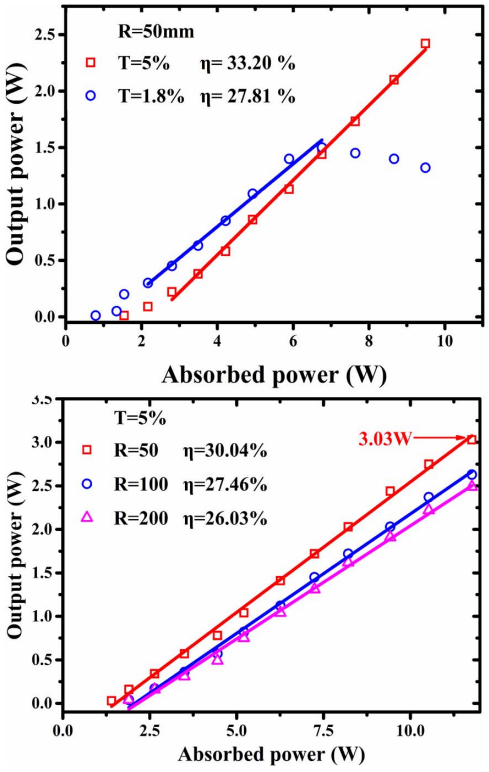

Fig. 3. (Top) 720.9 nm laser output curves of the 6-mm-long Pr:YLF crystal. (Bottom) 10-mm-long Pr:YLF crystal pumped by the 443.6 nm LD module.

The higher-order transverse mode caused by the thermal lensing resulted in serious mode mismatching. When the absorbed pump power exceeded 7 W, the output power began to descend, which should be attributed to mode mismatching.

For the 10-mm-long Pr:YLF crystal, the output power is also depicted in Fig. 3 (bottom). At the maximum incident pump power, the absorbed power without lasing was measured to be 11.98 W, corresponding to the absorption efficiency of 58.30%. OCs with a transmittance of 5% and different ROCs were used. For the OC with 50 mm ROC, the threshold absorbed power was 1.4 W, and the maximum output power of 3.03 W was obtained with a slope efficiency of 30.04%; the 720 nm laser was linearly polarized light in the π polarization direction. To the best of our knowledge, this is the maximum output power of Pr:YLF at 720.9 nm. One can see that the output power curves show no saturation, which means higher output could be expected if the pump can increase further. Another two OCs with 100 mm and 200 mm ROCs were used as well, but the threshold absorbed power increased, and the obtained maximum output power and the corresponding slope efficiency decreased as the ROC increased. The central wavelength of the deep red laser was 720.9 nm with an FWHM of 0.5 nm, as shown in Fig. 4.

For the 10-mm-long Pr:YLF laser, the far field patterns of the laser beam were recorded with a CCD and shown in Fig. 5. One can see that there was apparent distortion in the pattern when the laser operated at high power.

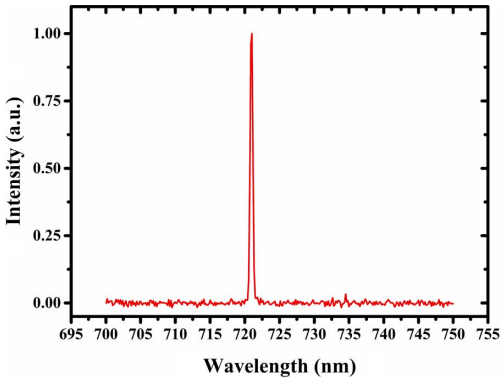

Fig. 4. Spectrum of the deep red laser at 720.9 nm.

Obviously, the distortion should be owing to the severe heat loading and relatively low thermal conductivity of the crystal. We numerically simulated the temperature distribution inside the crystal under the condition of 12 W absorbed pump power by finite-element analysis (FEA). The result of the numerical simulation is also shown in Fig. 5. The temperature difference between the center and the edge of the front surface was 77°C. Therefore, in order to obtain a higher quality transverse mode, better thermal management measures should be taken.

Up to now, 0.7 W deep red output with slope efficiency of 28.6% from a 3.5 W single LD pumped Pr:YLF laser was reported[31], but the crystal was cooled to 2°C. At room temperature, the maximum output power of 71 mW was produced when a 1.5 W single 444 nm LD was used as the pump source[11]. Nowadays, a single-emitter blue LD can emit 5 W output[12]. A single-emitter LD has obvious and considerable advantages in terms of price and volume compared with high-power fiber-coupled module or 2ω-OPSLs. Moreover, the single-emitter LD can possess a tight focus of pump, which is favorable to a low threshold. In our experiment, we found that the thermal effect became quite severe when using fiber-coupled LDs, so we tried the single-emitter LD pump source in order to obtain a high-power 720 nm laser at room temperature. The used pump source was a commercially available InGaN blue LD (Nichia Corp.) with maximum output power of 5 W and line width of about 1 nm (FWHM) at the maximum power. The beam quality factor M^2 of the pump beam

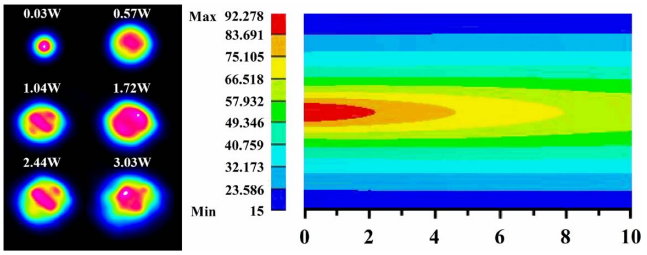

Fig. 5. (Left) Far field patterns of the laser beam recorded at different output power. (Right) Internal temperature distribution of 10-mm-long Pr:YLF crystal at 12 W absorbed power.

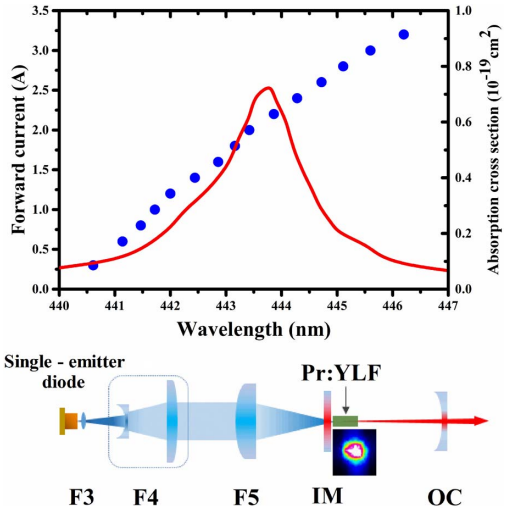

Fig. 6. (Top) Absorption spectrum of Pr:YLF at 444 nm and wavelength-shift of single-emitter LD. (Bottom) Schematic diagram of Pr:YLF laser pumped by a single 446 nm LD and pump beam pattern at the focus point.

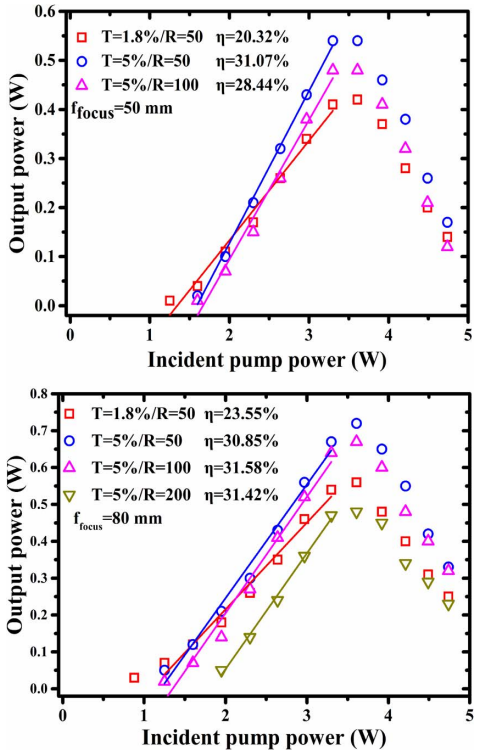

Fig. 7. Output characteristics of 10-mm-long Pr:YLF pumped by single 446 nm LD. (Top) Focal length is 50 mm; (bottom) focal length is 80 mm.

in the vertical and horizontal directions was calculated to be 1.42 and 13.1. The LD was fixed on a copper mount, which was cooled with 15°C circulating water. As shown in Fig. 6, the central wavelength of the LD drifts from 440.8 nm to 446.2 nm, when the forward current increases from 0.3 to 3.2 A. The schematic experimental setup is also depicted in Fig. 6. An antireflection coated (400–600 nm) aspheric lens F3 ($f = 4$ mm) and a pair of antireflection coated (400−700 nm) cylindrical lenses F4 ($f = -20$ and 100 mm) were used to collect and collimate the pump beam. The pump beam was coupled into the laser crystal that used a doublet F5, and the pump beam pattern at the focus spot is shown in Fig. 6 as well.

In order to improve the absorption efficiency of pump light, the 10-mm-long Pr:YLF crystal was used. Two doublets ($f = 50$ and 80 mm) were used to couple the pump beam into the Pr:YLF crystal. The characteristic of the output power is plotted in Fig. 7. When the 50 mm doublet was used, the size of the focus point was measured to be 37 μm × 35 μm, and three different OCs were used. The maximum output power was 0.54 W when an OC with an ROC of 50 mm and transmission of 5% was used, and the corresponding threshold incident pump power was 1.6 W. For the 80 mm doublet, the size of the focus point was about 59 μm × 55 μm, and four different OCs were used. The maximum output power of 0.72 W was obtained when an OC with a transmittance of 5% and an ROC of 50 mm was used, and the corresponding threshold incident pump power was 1.25 W. From Fig. 7, one can see that the OC with the transmission of 5% was more favorable for high-efficiency operation than the OCs with the transmission of 1.8%, which is the same as the above-investigated LD module pumping. Moreover, it is quite obvious that the laser performance improved a lot when the 80 mm doublet was used, which should be attributed to the better mode matching between the laser mode and pump mode. For the 50 mm and 80 mm doublets, the optimal cavity length was found to be 34 mm and 33 mm, and the beam waist of the laser mode in the cavity was 176 μm and 180 μm, respectively, by calculation of the ABCD matrix. The above calculation was based on the assumption of a −200 mm thermal lens focal length. Unfortunately, due to the LD's wavelength shift and the drawbacks of the heat sink, the pump wavelength has the highest overlap with the gain crystal absorption peak at the pump power of 3.6 W, as shown in Fig. 6. After this value was exceeded, the absorption efficiency of the pump laser by the crystal was significantly reduced, resulting in a significant reduction in output power.

In conclusion, a power-scaled Pr:YLF laser, operating at deep red wavelength of 720.9 nm, was reported. Two kinds of pump sources, one a 443.6 nm LD module and the other a single-emitter 446 nm LD, were used. When pumped by a 443.6 nm LD module, the laser generated the maximum output power of 3.03 W with a corresponding slope efficiency of 30.04%. When the laser was pumped by a single 446 nm LD, the maximum output power of 0.72 W was obtained with a corresponding slope efficiency of 30.85%, and higher output power was restricted by the wavelength mismatch between the pump wavelength and absorption band of the crystal. During the experiment, a crystal fracture occurred when the pump was tightly focused, and the beam quality was observed at different power levels. Currently, the maximum output power of the LD module has been increased to the hundred-watt level. Our results suggest that a new crystal cooling

scheme and/or double end pumping should be adopted to achieve high-power operation of Pr:YLF visible laser in the case of high-power pump.

This work was supported by the National Natural Science Foundation of China (Nos. 61405126 and 61704112), the Science and Technology Planning Project of Shenzhen Municipality (Nos. ZDSYS201707271014468 and JCYJ20170817094438146), and the Educational Commission of Guangdong Province (No. 2016KCXTD006).

References

1. C. Krankel, D. T. Marzahl, F. Moglia, G. Huber, and P. W. Metz, Laser Photon. Rev. **10**, 548 (2016).
2. A. Kamrnskii, H. J. Eichler, B. Liu, and P. Meindl, Phys. Stat. Sol. (a) **138**, K45 (1993).
3. T. Sandrock, T. Danger, E. Heumann, G. Huber, and B. H. T. Chai, Appl. Phys. B **58**, 149 (1994).
4. A. Richter, E. Heumann, E. Osiac, G. Huber, W. Seelert, and A. Diening, Opt. Lett. **29**, 2638 (2004).
5. V. Ostroumov, W. Seelert, L. Hunziker, C. Ihli, A. Richter, E. Heumann, and G. Huber, Proc. SPIE **6451**, 645103 (2007).
6. M. Fibrich, H. Jelínková, J. Šulc, K. Nejezchleb, and V. Škoda, Proc. SPIE **7578**, 757828 (2010).
7. T. Gün, P. Metz, and G. Huber, Opt. Lett. **36**, 1002 (2011).
8. P. W. Metz, K. Hasse, D. Parisi, N.-O. Hansen, C. Kränkel, M. Tonelli, and G. Huber, Opt. Lett. **39**, 5158 (2014).
9. P. W. Metz, F. Reichert, F. Moglia, S. Müller, D.-T. Marzahl, C. Kränkel, and G. Huber, Opt. Lett. **39**, 3193 (2014).
10. H. Tanaka, R. Kariyama, K. Iijima, K. Hirosawa, and F. Kannari, Opt. Express **23**, 19382 (2015).
11. E. Damiano, J. Shu, A. Sottile, and M. Tonelli, J. Phys. D: Appl. Phys. **50**, 135107 (2017).
12. H. Tanaka, S. Fujita, and F. Kannari, Appl. Opt. **57**, 5923 (2018).
13. B. Xu, P. Camy, J.-L. Doualan, Z. Cai, and R. Moncorgé, Opt. Express **19**, 1191 (2011).
14. B. Xu, Z. Liu, H. Xu, Z. Cai, C. Zeng, S. Huang, Y. Yan, F. Wang, P. Camy, J. L. Doualan, A. Braud, and R. Moncorgé, Opt. Commun. **305**, 96 (2013).
15. S. Luo, X. Yan, Q. Cui, B. Xu, H. Xu, and Z. Cai, Opt. Commun. **380**, 357 (2016).
16. N. Niu, S. Pu, Q. Chen, Y. Wang, Y. Zhao, W. Wu, and Q. Zheng, Appl. Opt. **57**, 9798 (2018).
17. M. Fibrich, H. Jelínková, J. Šulc, K. Nejezchleb, and V. Škoda, Laser Phys. Lett. **8**, 559 (2011).
18. M. Fibrich and H. Jelínková, Laser Phys. Lett. **10**, 035801 (2013).
19. X. Lin, X. Huang, B. Liu, B. Xu, H. Xu, Z. Cai, X. Xu, D. Li, J. Liu, and J. Xu, Opt. Mater. **76**, 16 (2018).
20. A. Sottile, Z. Zhang, S. Veronesi, D. Parisi, A. D. Lieto, and M. Tonelli, Opt. Mater. Express **6**, 1964 (2016).
21. S. Zhou, Y. Pan, N. Li, B. Xu, J. Liu, Q. Song, J. Xu, D. Li, P. X. Xu, and J. Xu, Opt. Mater. **89**, 14 (2019).
22. S. Sattayaporn, P. Loiseau, G. Aka, D.-T. Marzahl, and C. Kränkel, Opt. Express **26**, 1278 (2018).
23. F. Varsanyi, Appl. Phys. Lett. **19**, 169 (1971).
24. E. Balanikas, A. Banyasz, G. Baldacchino, and D. Markovitsi, Molecules **24**, 2347 (2019).
25. F. Torche and J. L. Marignier, J. Phys. Chem. B **120**, 7201 (2016).
26. A. Diaspro, D. Silvano, S. Krol, O. Cavalleri, and A. Gliozzi, Langmuir **18**, 5047 (2002).
27. Q. Wu and H. Xu, Food Chem. **290**, 24 (2019).
28. G. Huber, A. Richter, and E. Heumann, Proc. SPIE **6451**, 645102 (2007).
29. X. Peng, L. Xu, and A. Asundi, Appl. Opt. **44**, 800 (2005).
30. V. V. Zelenogorskii and E. A. Khazanov, Quantum Electron. **40**, 40 (2010).
31. Y. Zhang, Y. Yang, L. Zhang, D. Lu, M. Xu, Y. Hang, S. Yan, H. Yu, and H. Zhang, Chin. Opt. Lett. **17**, 071402 (2019).